EUROPEAN ORGANIZATION FOR NUCLEAR RESEARCH

CERN/EF 84-9
20 June 1984

HOLOGRAPHIC RECORDING OF COSMIC RAY TRACKS IN BEBC

H. Bjelkhagen(*), G. Harigel(**), F. Pouyat, W. Seidl,
CERN, Geneva, Switzerland

C. Baltay, M. Bregman, F. Eisler(***), M. Hibbs, A. Schaffer,
Columbia University, Nevis Laboratories, Irvington, N.Y. 10533, USA

R. Cence,
Department of Physics, University of Hawaii at Manoa,
Honolulu, Hawaii 96822, USA

E.B. Brucker, T.J. Hart,
Department of Physics, Stevens Institute of Technology,
Hoboken, N.J. 07030, USA

ABSTRACT

We report on a successful test of holography in the Big European Bubble Chamber (BEBC) at CERN, which was filled with a heavy neon-hydrogen mixture. During the test of a modified in-line scheme we photographed bubble tracks longer than 1 m, which were produced by cosmic rays. The smallest bubbles, which were recorded with excellent contrast, had a diameter of $\gtrsim$ 100 μm. This presents an improved resolution of more than a factor of five compared to photos taken with conventional cameras.

Submitted to Nuclear Instruments & Methods

(*) Permanent address: Royal Institute of Technology, Division of Production Engineering, S-10044 Stockholm 70, Sweden

(**) Also at Columbia University, Nevis Laboratories, Irvington, NY, USA

(***) College of Staten Island, CUNY, Staten Island, NY 10301, USA

EF/1415F/GH/ef

1. INTRODUCTION

In recent years there has been increased interest in high-resolution track detectors to be used to detect the short-lived charmed particles and the τ lepton. These particles have such short lifetimes that even at very high energies they typically travel only a few millimeters between production and decay. In order to identify such particles and measure their lifetimes one requires high enough resolution to be able to clearly identify both the production and decay point.

Recently a number of groups have developed small high-resolution bubble chambers to be used as vertex detectors in association with larger electronic detectors. These groups have demonstrated that holography is a practical way to achieve the highest spatial resolution possible [1,2].

The applicability of holographic techniques to big bubble chambers was already proposed before 1970 by W.T. Welford [3] and collaborators, and the idea was revived in a theoretical article by F. Eisler [4]. Lately, some groups have been trying to work out schemes for BEBC at CERN and for the 15-Foot Bubble Chamber at Fermilab [5,6]. At present the resolution of these chambers is limited to $\gtrsim$ 500 μm by the conventional optics used to photograph in bright-field illumination the bubble tracks. In order to achieve much higher resolution with conventional optics one is forced to give up depth of field, thereby reducing the usable volume of the chamber [7], certainly undesirable for neutrino physics. One possible solution is to use holography to supplement the conventional optics. Holography holds the promise of a considerable improvement in resolution throughout a large depth of field, however the width of view being limited by the coherence length of the laser beam. A hologram records optically a volume in such a way that objects at all positions within the volume can be reconstructed in perfect focus.

In the present paper we describe the experimental set-up for a modified in-line holographic scheme, which was developed by C. Baltay et al. [8]. We present results from photographing test objects with BEBC still empty and of bubble tracks in a neon-hydrogen mixture produced by cosmic rays.

Requirements on the laser beam coherence length, pulse length and Gaussian profile, mainly in view of future applications in the Fermilab 15-Foot Bubble Chamber for Tevatron neutrino and beam dump exposures, and the necessary laser energy to illuminate a large fraction of its fiducial volume of about 18 m^3, are discussed. During the test it became apparent that heating effects by the high-energy laser beam produces boiling in the neon-hydrogen which spoils the quality of the conventional photographs and the thermodynamics during and after the chamber expansion. Ideas to limit or prevent this parasitic boiling are presented. Methods for reconstruction of the holograms (in combination with the conventional photos) are being compared.

2. DESCRIPTION OF THE METHOD

A hologram is formed by the interference of coherent light from a reference beam with the coherent light scattered by an object.

Small bubble chambers have been designed such that the reference beam and the object beam, of sufficiently large diameter, are either identical and going through the same liquid volume (in-line holography), or that the reference beam (a small fraction of the total beam separated by a beam splitter) goes directly onto the photographic emulsion and does not enter the medium which is traversed by the remaining larger beam intensity (two-beam holography).

Large bubble chambers were not designed for the application of holography and it would be difficult to simply scale the techniques applied in small chambers. Therefore, some compromises had to be made. We describe here the principle features and the experimental scheme, in which the object and reference beam are combined in a modified in-line set-up.

A powerful laser beam enters the bubble chamber through a small window at the bottom of the chamber. This beam is then diverged by a specially designed aspheric lens such that only a small part of the light goes directly through the center of a fisheye window onto the film (reference beam), and the rest illuminates the bubble chamber tracks

within a large conical volume. The intensity of this illuminating beam at large angles increases to compensate for the decrease of the light scattered by the bubbles at large angles.

Our system may be best explained by first considering bubbles, which are close to the optical axis of the system. Laser light of intensity E_{inc} [ergs/cm^2] and wavelength λ illuminates a bubble of diameter d. The total energy that hits the bubble is $E_{inc} \times \pi (d/2)^2$. This scattered coherent light is contained in a diffraction spot of radius $\delta = 0.77 (\lambda/d) \times D$, where D is the distance away from the film. The intensity of the scattered light of the film is then

$$E_{scatt} = E_{inc} \times \pi(d/2)^2/\pi\delta^2 = E_{inc} \times \frac{D^4}{4\lambda^2 D^2} \quad \frac{1}{0.77^2} .$$

The intensity distribution on the film will be an interference pattern due to the bubble scattered light and the coherent reference beam

$$I \text{ (film)} = \vec{A}^2_{ref} + 2\vec{A}_{ref} \times \vec{A}_{scatt} + \vec{A}^2_{scatt} ,$$

where the A's are the amplitudes of the scattered and reference beams, respectively, and $E_{scatt} = A^2_{scatt}$ and $E_{inc} = A^2_{ref}$. The modulation of the inteference pattern, is related to the beam balance ratio, which is

$$BR \simeq \frac{2\vec{A}_{ref}\vec{A}_{scatt}}{\vec{A}^2_{ref}} \simeq \frac{2\vec{A}_{scatt}}{\vec{A}_{ref}}$$

and is proportional to the amplitude ratio. So, in this case,

$$BR = \frac{2\vec{A}_{scatt}}{\vec{A}_{ref}} = \left\{\frac{E_{scatt}}{E_{inc}}\right\}^{1/2} = \frac{d^2}{2\lambda D} .$$

We see from this expression that as we increase the distance to the film D we have to keep d^2/D constant to keep the same beam balance ratio. We need, in a big bubble chamber, a minimum bubble diameter of 75 μm, when the distance D of the bubble to film is 200 cm (λ = 0.694 μm) and BR = 10^{-3}, as has been established in small bubble chambers.

The resolution of this technique is given by the expression

$$\delta = 0.77 \frac{\lambda}{n \cdot a\ (film)} \times D \ ,$$

where a (film) is the diameter of the hologram and n is the index of refraction of the bubble chamber medium. Neglecting the adverse effects of the fisheye windows, and taking for our case $\lambda \sim 0.694$ μm, a(film) ~ 70 mm, and the median plane D = 200 cm, we expect a resolution of 29 μm in space, which is sufficient to photograph 75 μm bubbles.

Since we want to illuminate as much as possible the fiducial volume of a big chamber to study in detail event vertices, the laser light will be spread into a cone of 40° half angle. Then the hologram is the interference between the reference beam, which is just the unscattered light wave from the laser to the film, and the light wave scattered by the bubbles. The main problem in this scheme is that light must be scattered by the bubbles at large angles α, in the range $0 < \alpha < 60°$, to cover most of the fiducial volume. The amount of light scattered by a spherical bubble at large angles is given in an article by Welford [9] to be

$$E_{scatt} = E_{inc} \times \left(\frac{r^2}{D^2}\right) G(\alpha) \ ,$$

where E_{scatt} is ergs/cm^2 at a distance D from the bubble, E_{inc} is ergs/cm^2 hitting the bubble, r is the radius of the bubble in centimetre, G(α) is determined by the scattering cross section which changes rapidly with the scattering angle α and is shown in fig. 1. To compensate for this rapidly falling G(α) we spread the laser light out non-uniformly, so that we have much higher intensities at large angles. For example, on axis we would have 10 ergs/cm^2 which is what we need for the reference beam to correctly expose a commercially available non-specially treated film (e.g. AGFA 10E75(*)). Near the edge of the chamber where G(α) is small, we would have 10 000 ergs/cm^2 so that we would keep E_{inc} xG(α) and therefore E_{scatt} approximately constant. This requires a nonspherical diverging lens.

(*) This exposure is needed due to the reciprocity behaviour of the material when applying a Q-switched laser pulse.

3. THE EXPERIMENTAL ARRANGEMENT

The test of the in-line holography in BEBC required little modifications on the chamber in order to be compatible with the hydrogen safety code, and not to perturb a physics run. These requirements dictated to a large extent the experimental set-up, as shown in fig. 2.

A ruby laser (described in more detail below), consisted of an oscillator stage and four amplifiers, mounted horizontally on a precision optic bench, was installed in the expansion pit underneath BEBC in a pressurized porta-camp. The laser beam was reflected by a dielectric mirror straight upwards through a vacuum tank window and two other windows (in an existing flange) on the chamber into its interior. The flat windows were made out of quartz (Homosil), had a thickness of 20 mm and a diameter of 100 mm on the vacuum tank and 80 mm on the chamber. In order to prevent condensation of gases or oil, particularly on the cold windows, a tube was installed between the warm and cold windows, having a separate vacuum system and equipped with a cold trap. Inside the chamber the beam was deflected by 34° by another dielectric mirror towards one of the five fisheye windows on top of the chamber vessel. The diverging lens (described below) was rigidly attached to this mirror; with its optical axis pointing at the fisheye. The film platen was inside the centre of the smallest hemispherical window, almost perpendicular to the laser beam, except for a remaining tilt of 7°. The film transport in this holographic port was a modified version of the standard BEBC camera, but without the wide angle lens.

3.1 The ruby laser

The ruby laser (KORAD K-1000 Ruby Laser System, λ = 694.3 nm) was given to us by Columbia University's Radiation Laboratory. It consists of an oscillator stage and two amplifiers, and had, in its conventional multimode operation, a nominal output of 40 J with a pulse duration of 1 ms. For our application we operated the oscillator stage in the Q-switched and in transverse TEM_{oo}-mode, giving a single-mode ~ 20 ns pulse (rise time 10 ns) with a Gaussian-like spatial intensity distribution. This produces a long coherence length and no mode beating. Operation in this mode reduces the output of the oscillator to such an extent, that four more amplifiers were needed to obtain a maximum output of 7 J. This was

sufficient for illuminating a cone of 20° half angle inside BEBC. The repetition rate of the laser was two pulses per minute, and was determined mainly by the charging time of the capacitor banks for the flash lamps.

Fig. 3 shows the entire set-up on a 4 m long optical bench, the dimensions of the various ruby rods are given in the figure caption. The last rod had at its downstream end a Brewster angle cut to prevent possible damage to the whole system by unwanted reflections back into the oscillator. A 45° quartz prism was used to return the beam parallel to the optic axis of the oscillator. The beam expanding optics were adjusted to fill the ruby rods, so as not to exceed a peak power level of 300 MW/cm^2, which could damage the rods, and to give flexibility in illuminating various diameters of the light diverging lens inside the chamber.

3.2 The aspheric diverging lens

The aspheric diverging lens was manufactured out of quartz (Herasil Top), had an outside diameter of 60 mm, an effective diameter of 50 mm and a thickness of 35 mm.

The aspheric surface was calculated with a computer program, taking into account the refractive index of quartz (n_Q = 1.455) and of 70/30 mole percent neon/hydrogen at a temperature of about 30 K (n_{Ne} = 1.085). The main parameter was the desired beam balance ratio, which is critically influenced by the curvature of the central part of the lens.

Fig. 4 shows the theoretical input curve for light intensity as function of the divergence angle together with the experimental measured in air. Fig. 5 shows the measured angle of the light cone as function of the illuminated front diameter of the lens. The drop in intensity along the axis follows a $1/r^2$ law.

3.3 Auxiliary equipment

One of the BEBC standard cameras was modified so that the 70 mm holographic film (with a modified standard perforation (only 1 hole punched out of 4)) could be transported down to the centre of the fisheye

window. This film, which has a thick (170 μm) and rigid support base had to be kept perfectly flat on the film platen with vacuum suction.

Due to the high power of the laser, all flat entrance windows had to be manufactured out of quartz, which can stand thermal shocks considerably better than ordinary glass. These windows had antireflection coating optimized for ruby laser light and were optically very homogeneous. Mirrors were multilayer dielectric coatings (manufactured by Matra and Balzers) on quartz slabs.

4 EXPERIMENTAL RESULTS

4.1 Operation of the ruby laser

For our application the requirements on the performance of the ruby laser system are extremely high. The quality of the holograms depends heavily upon the coherence length, the time structure of the laser beam, the spatial light distribution, the centring of the beam on the aspheric lens, and sufficient and stable output energy.

4.1.1 Measurement of the coherence length

The temporal coherence of any spectral source is defined as the path length difference over which the radiation can still interfere with itself.

There are various methods to measure the time width of the laser emission. We choose the purely optical technique (holography), which is the most sensitive method to study the longitudinal modes of the pulsed laser.

For this holographic test an object 80 cm long was illuminated by the laser through a negative lens with short focal length (fig. 6). The object, positioned in the direction of the beam, slightly tilted, was covered by a retro-directive tape (Scotchlite) and was marked every 10 cm. At the distant end of the bar a mirror (4% reflectivitiy) was positioned creating the reference beam. This mirror directed the beam towards a second mirror (100% reflectivity), which in turn directed the reference beam towards the film. This holder was installed very close to the illuminating lens in order to utilize the retro-reflecting property

of the Scotchlite bar. At a special point on the bar (slightly behind the 4% mirror) the path lengths for the reference beam (via the two mirrors) and the object beam are equal. This point is bright even if the coherence length is poor. The holographically measured length in front of that point indicates the fringe-free distance that is obtainable in the hologram and thus gives the coherence length of the laser.

Holograms were recorded for different voltage settings of the capacitor bank for the oscillator, various delays of the Pockel cell, and the temperature of the etalon. Recordings were also made at identical settings to study the pulse-to-pulse stability of the laser. After development of the film the holograms were reconstructed by means of a helium-neon gas laser. The coherence length was measured visually by observing the fringe-free part of the bar in the hologram. A photograph of such a recording is shown in fig. 7.

We obtained coherence lengths of ~ 200 to 300 mm with very good stability and sometimes, although not reproducibly, up to 500 mm with the following settings:

Oscillator voltage (near threshold)	3.8 - 3.9 kV
Pockel cell voltage	8.0 kV
Pockel delay	1.1 ms
Temperature of output etalon	24.2°C
Temperature of invar cage	19.3°C
Aperture	1.8 mm

Variations around these indicated values resulted in the following observations:

(a) An increase of the oscillator voltage results in a rapid decrease of the coherence length.

(b) Variations of the Pockel cell voltage and its time delay has very little effect.

(c) Any variation of the temperature of the output etalon of ± 0.2°C or greater reduced the coherence length.

(d) Variation of the temperature of the invar cage (length of the cavity) by a few tenth of a degree has no effect.

(e) The aperture size, varied from 1.5 to 3.5 mm, has very little effect on the spatial coherence. However, as will be explained below, the aperture size had a strong influence upon the TEMoo-mode.

4.1.2 Transverse mode selection

A Gaussian beam profile is used as input into the design of the light diverging and needed to obtain good spatial coherence.

The distribution of power density in a beam with the fundamental or TEM_{oo}-mode is

$$I(r) = I_o \exp\left(\frac{-2r^2}{\omega^2}\right) ,$$

where r is the distance from the axis in the Gaussian beam and ω is the radial distance at which the field amplitude drops to 1/e of its on-axis value and thus the power density is decreased to $1/e^2$ of its axial value.

Transverse-mode selection is generally achieved by using an aperture inside the cavity of the oscillator. In general, the size of the aperture in a 75 cm long cavity has to be between 1.5 - 2.0 mm to achieve the TEM_{oo}-mode. Several experiments were performed to try different diameters and different positions of the aperture as well as different resonator mirrors.

An optimal combination was found using an aperture of 1.5 mm. Sometimes, bigger apertures were used (1.8 - 2.0 mm) in order to increase output power.

4.2 Holograms in empty BEBC

The properties of the entire experimental arrangement were first tested at ambient temperature in air, when the interior of BEBC was still accessible. Nylon wires with various diameters (mainly Ø = 100 µm) were suspended inside the chamber vessel. A more refined target, consisting of a square plastic frame (15 x 15 cm^2), was the holder for glass beads (Ø = 100 µm), which were glued onto 20 µm wires. The picture of this target, taken with an ordinary camera in the laboratory, is shown in fig. 8(a); the distance between the two parallel wires is 3 mm. Glass beads are the best way to simulate bubbles in liquid neon-hydrogen when they are seen under an angle of 10° with respect to the axis of the reference beam, and when they are positioned half way between the

light-diverging lens and the film. Then the scattering angle is $\alpha = 20°$ (compare fig. 1). The target was photographed holographically in BEBC, off-axis and 2 m away from the lens. The lens was illuminated by a parallel beam with a diameter of 1.5 cm, a laser energy of ~ 6 J, sufficient for a cone with a half angle opening of 15° (compare fig. 5). We obtained excellent photos inspite of the fact, that the coherence length (only a few millimetres) was not yet optimized. For this test the oscillator stage had a curved back mirror (radius = 2000 cm), an etalon acting as front mirror (reflectivity $\gtrsim$ 4%) an aperture of 1.6 mm and the voltage setting was close to the threshold for lasing (U = 4.65 kV). The hologram was replayed in a time-reversed beam through a fisheye set. Only a few square centimetres out of ~ 50 cm^2 of the hologram were illuminated by an argon laser to suppress abberations (sect. 5) (λ = 514.5 µm, E = 5 W in multi-mode, 1 W in single-mode). The real image was then taken on a photographic plate at the point of best focus and is shown in fig. 8(b). These tests demonstrated that the method worked satisfactorily, and gave a first indication of obtainable resolution.

4.3 Operation of the bubble chamber

BEBC, filled with a 70/30 mole percent neon-hydrogen mixture was operated in the usual way, i.e. at a liquid temperature of 29.4 K, a static pressure of 8.6 bar, a piston stroke of 6.4 cm, resulting in a pressure drop of 3.2 bar. The expansion cycle had a duration of ~ 100 ms, and the chamber was pulsed every 4 s. The magnetic field was 3.5 T.

Fig. 9 shows schematically the dynamic pressure curve, the time of particle injection and the firing of the flash lamps for the conventional cameras 10 ms later. The delay for the laser pulse was chosen to be 2 ms, i.e. 8 ms prior to the normal pictures. These delays will be characteristic for future experiments using holography in conjunction with regular photos. The intention is to record holograms when the track bubbles are still fairly small and their density has not yet been diminished by the growing together of neighbouring bubbles, whereas the timing for conventional pictures provides standard size bubble tracks for scanning and curvature measurements.

Since BEBC was being run during the holographic tests for a neutrino oscillation experiment at PS-energies, the interaction rate was extremely low (about one interaction in a thousand frames). Therefore, we had to rely on photographing cosmic ray tracks appearing at random (times and places) in the chamber. They are abundant: during the sensitive period of ~ 15 ms about a dozen cosmic rays traverse the fiducial volume, mostly vertically. Thus, we had to cope with a large variety of bubble sizes and densities.

4.4 Holograms of bubble tracks

After the alignment of the laser beam on the centre of the vacuum tank window, holograms were taken with various energies and beam diameters. The oscillator stage consisted out of a flat back mirror (100% reflectivity), the Pockel cell, followed by a diaphragm (1.5 or 1.8 mm), the oscillator ruby rod (3/8" diameter), a 4-plate uncoated etalon and a flat front mirror (70% reflectivity). The oscillator voltage was set to 4.8 kV, the amplifiers were powered with maximum voltage (~ 5.0 kV), and this resulted in an output energy of ~ 2 or ~ 3.5 J for the two apertures, respectively. No systematic and precise measurements of the beam profile were made. From burn patterns taken immediately after the oscillator, the last amplifier and below the vacuum tank we found qualitatively that we never obtained a Gaussian light distribution in the far field. In particular, the burn pattern below the vacuum tank had the appearance of a TEM_{01}*-mode. The burn patterns gave information about the beam divergence. This was important since focusing of the beam on the chamber windows had to be avoided for safety reasons. Deviations from a Gaussian profile did not seem to affect the quality of the holograms to any obvious degree. Pulse-to-pulse variations in the quality of the holograms can probably be attributed to some accidental non-stationary obstruction in the light passing inside the liquid between the entrance window and the aspheric lens. This obstruction did not allow us to determine an optimum beam balance ratio, nor to fix precisely, the necessary laser energy for a given illuminated volume. The precision of calorimeter measurements of the output energy of the laser was limited due to the presence of the stray field (~ 300 G) from the chamber magnet.

It is difficult to determine the absolute diameter of a bubble because it is surrounded during the growth process (expansion) with a cold

layer and during its recondensation (recompression) with a warm layer of liquid of changing thickness, and varying refractive index. This difficulty is present for dark and bright-field illumination, including any sort of holographic recording. Furthermore, the image size depends on exposure and development of the film. In general, images are measured with a microdensitometer on film and the full width at half maximum is quoted as bubble diameter. The difference of optical density between the background and the centre of the bubble image should be ~ 0.8 to show good contrast. Bubble tracks from the replayed hologram (for replay technique see sect. 5) are shown in figs 10(a-d). Bubbles are measured from the photograph (fig. 10(a)) with a microdensitometer and results are shown in figs. 11(a-b). The scaling from film to bubble chamber takes into account the difference in wavelength of the ruby laser for the exposure and the argon laser used for the replay, as well as the difference in refractive indices of the liquid and of air. Bubbles with $\lesssim$ 120 μm diameter FWHM (fig. 11(a)) can be seen with excellent contrast, and the two-bubble resolution is ~ 200 μm (fig. 11(b)). Bubble centers can probably be measured with a precision of ~ 30 μm. Figs 10(c-d) give a comparison between the same track once replayed from the real image and once from the virtual image, the latter from the TV screen presentation.

The illuminated light cone was $\lesssim$ 20° half angle, and tracks having lengths $\gtrsim$ 1 m could be seen up to regions close to the fisheye windows Variations in quality of bubble images along the track may be attributed primarily to the limited coherence length and a non-perfect illumination.

Resolution and contrast can be improved by both, better laser operation and more refined replay techniques. Therefore, the present results obtained from an arbitrarily selected cosmic ray track sample should be taken as a feasibility test rather than an obtainable limit for this new technique.

Energy requirements for illuminating a cone with 40° half angle, instead of 20° during our present test, can be estimated theoretically on the basis of the design of the light diverging lens and the scattering function of bubbles. Such an estimate results in the need of a more than an order of magnitude increased laser energy. However, absolute values for such a large cone will not be given at this time, since we could not

determine, to sufficient accuracy, the beam balance ratio. We only recently investigated the possibility to hypersensitize film by various methods. Effects arising from stretched laser pulses, which have influenced the emulsion sensitivity (reciprocity behaviour) are described elsewhere [16]).

4.4.1 Interference between the light sources

Holograms and conventional pictures could not be taken together during the same bubble chamber expansion, since the stray light from the flash tubes produced an unacceptable level of fogging on the holographic film (AGFA 10 E 75). Therefore, we always took a few holograms, and then some conventional pictures during following expansions. In the future this interference problem can be cured either by putting a filter (or shutter) in front of the holographic film and, if necessary, a filter in front of the flash tubes, which cuts off light at the red end of the spectrum.

The stray light from the laser did not disturb to any significant amount the conventional photographs (film 3M 921).

4.4.2 Laser-induced parasitic boiling

A problem arises from the interaction of the laser beam with the bubble chamber liquid or with its microscopic impurities. This laser light produces bubbles which continue to grow and eventually obstruct the conventional photos to such an extent, that bubble tracks disappear in a foggy background. Since the growth of the embrionic laser induced bubbles is negligibly small during the short laser pulse itself, the holograms remain unaffected by these miniscule bubbles (diameters probably $\lesssim 0.2$ μm). However, another disturbance comes from the recompression of these bubbles which starts about 15 ms later. By then they have obtained sensible sizes and the irreversible heat produced disturbes the overall temperature stability of the chamber. When produced in large quantities, the effect of these bubbles upon the dynamic pressure curve is visible on the oscilloscope pictures (figs 12(a-b)) showing an instantaneous pressure increase of 0.25 bar during recompression. These bubbles appear to grow significantly slower than track bubbles: this may be attributed to their high density, preventing the fast extraction of heat for vaporization from

their vicinity. A picture of this bubble cone, taken with cameras 1, 3, 4 and 5, is shown as fig. 13. This bubble cone, however, provided a means to check the size and the direction of the laser illumination and also roughly the beam position of the front side of the aspheric lens. Fig. 13 shows for example that during this particular pulse the beam was not well centred on the lens giving an imperfect asymmetric light cone pointing not exactly to optic port No. 2. The streaky structure inside the bubble cone can be attributed to self-focusing effects of the laser at high power densities and/or to imperfections of the diverging lens.

Light induced bubbles have been studied in bubble chambers filled with various liquids [10-12]. All authors assume that light absorption on microscopic, partially or non-transparent impurities is responsible for bubble nucleation rather than ionization of the liquid via multiphoton processes. Further hints for the validity of this interpretation comes from the fact that the sensitivity to laser light stretches far into the region of low temperatures [10], where chambers are no longer sensitive to ionizing particles, and that it is wavelength independent throughout the visible spectrum [11].

It is difficult to relate the results quantitatively on to one common denominator since liquids, operating conditions, and possibly also the size of impurities differ appreciably. However, if the general interpretation is correct, the number of bubbles should drop with a reduction of the laser power at constant energy, i.e. when the laser pulse is stretched in time. In a scatter plot we show the results from these experiments and the recent tests in BEBC as function of laser energy versus its pulse duration (fig. 14).

For BEBC we had the advantage that we could operate the laser with either 20 ns or 1 ms pulses under the same chamber conditions. We did not find any boiling when the pulse was 1 ms long, even at slightly increased energy. Observations were made in two regions of the chamber:

(a) in a small gap just visible underneath the aspheric lens, where the laser light is still parallel and the energy density is reasonably well known;

(b) near the border region of the light cone ~ 2 m away from the lens, where the energy density is known only approximately.

Disregarding the result from ref. [12] we can then estimate the position of a line in the scatter plot, which separates regions where boiling is expected and where it is not. This interpretation leads to the conclusion, that stretching of the laser pulse to ~ 1 μs would permit, for our envisaged application in big chambers, higher laser energies and consequently a larger illuminated cone without boiling. We expect that such a pulse duration is still tolerable: mechanical vibrations during the expansion (main frequency in BEBC 40 Hz, 120 ms cycle duration in Ne/He [13]), bubble movement due to buoyancy forces (< 150 nm [14]) and change of bubble diameter due to their growth (~ 2 μm [15]) should not affect the good quality of the holograms of particle tracks. If a small amount of laser-induced bubbles should still be present, their sizes (~ 2 μm) would probably not trouble the holograms. However, they may then grow like ordinary track bubbles and cause minor disturbance on the conventional pictures.

Extension of the laser pulse, while still maintaining its long coherence length could solve, at least, a part of the problem. In addition, the use of various methods to increase the sensitivity of the film [16] would allow for reduction of the input energy from the laser. The option of using the 20 ns pulse for tests of the direction of the light cone via bubble creation should be kept.

Some parasitic boiling existed during the test run around the aspheric lens and may have affected the quality of the holograms given rise to occasionally observe double images of tracks. This boiling can be avoided in a final design by putting the aspheric lens outside the chamber, just behind a flat window on the chamber.

4.4.3 The magnetic field

All secondary effects on the power supplies from the magnetic stray field (~ 300 G) at the location of the laser were quickly overcome.

Linearily polarized light will be subject to the Faraday effect when it passes through a magnetic field. Assuming the Verdet constant to be

similar in liquid hydrogen and liquid neon/hydrogen (~ 5.10^{-3} min/G • cm), we expect in the BEBC field of 3.5 T and a path length of the light of some 400 cm in the liquid and 9 cm in glass and quartz that the polarization would be rotated by more than 3 complete revolutions. However, the rotations depend on B • ℓ (ℓ is the path) and both the reference beam and the scattered beam have to a good approximation the same B • ℓ. We did not observe any adverse effect within the light cone of 20° half angle.

5. REPLAY SCHEMES FOR HOLOGRAMS

Holograms in BEBC were taken through a set of three hemispherical windows (fisheye windows, f = -300 mm). Therefore it appears to be convenient to replay these holograms through the same or at least a similar set of windows. In the replay one can either look at the real image with a "time-reversed" beam, or at the virtual image by reproducing the illumination beam from the bubble chamber set-up. Both methods suffer from the fact, that the refractive index of liquid neon-hydrogen cannot be simulated easily and that in general the wavelengths of the pulsed beam for the exposure and the continuous laser beam for the replay are not identical. In addition, the replay of the real image requires a room of the size of the bubble chamber. To overcome these difficulties a holographic measuring machine using the real image is being built in Hawaii [17]. By using a clever system of adjustable mirrors and by rotating the hologram the real image can always be brought to the same point in space. It can then be displayed on a TV monitor using a Vidicon tube which can remain at a fixed position. There are four sources of distortion which must be taken into account:

- the effect of the fisheye aberrations on the reference beam,
- the effect of the fisheye aberrations on the scattered light,
- the index of refraction of the bubble chamber liquid,
- and the difference and wavelength between the laser used to make the hologram and the laser used to replay it.

A system of spherical lenses is designed bracketing the hologram which compensates for all of the above aberrations satisfactorily if only

the central 50 cm of the hologram is illuminated. This would include about half of the available area. The current design calls for the use of an air bearing in order to digitally rotate the hologram accurately enough so that positions can be measured in space with an error of ~ 10 μm for an image distance of 2 m.

The virtual image has the advantage that it is brighter and the disadvantages that it is smaller and distorted. Thus, measurements need to be more precise. With the addition of a single fixed telescope the virtual image could be used if this turns out to be more advantageous.

In both schemes it is easier to obtain good coordinate readings in the x,y-plane (perpendicular to the reference beam), than in the z-direction, where one has to rely on the judgement of best focusing. The two replay techniques are shown very schematically in fig. 15.

Other approaches to replay holograms from a big bubble chamber are being studied.

The scaling law for the different wavelength, used during taking the hologram (λ_1) and replaying it (λ_2), and employed during the BEBC test, is [18]

$$z_i = \left\{ \frac{1}{z_p} - \frac{\lambda_2}{\lambda_1 z_r} \pm \frac{\lambda_2}{\lambda_1 z_o} \right\}^{-1},$$

$$x_i = \mp \frac{\lambda_2 z_i}{\lambda_1 z_o} \cdot x_o \pm \frac{\lambda_2 z_i}{\lambda_1 z_r} \cdot x_r + \frac{z_i}{z_p} \cdot x_p ,$$

and a corresponding expression for the other coordinate perpendicular to the optical axis y_i, where

z_r = distance from light diverging lens to film (in chamber),
z_p = distance from light diverging lens to film (in replay),
z_o = distance from bubble to film (in chamber),
z_i = distance from bubble to film (in replay),

and

x_o, y_o = distance of bubble from optical axis (in chamber),
x_i, y_i = distance of bubble from optical axis (in replay),
x_r, y_r = 0
x_p, y_p = 0 } when a time reversed beam is used.

The upper sign in above formulas refers to the virtual image, the lower sign to the real image.

The ratio of the refractive indices in liquid and in air affects only the calculation of the depth coordinate z.

6. CONCLUSIONS AND OUTLOOK

We have demonstrated that bubble tracks can be photographed with a modified in-line technique in large bubble chambers and replayed with good contrast and a resolution, at least five times that of conventional bright-field pictures. No adverse effects of the magnetic field upon holography were observed during our test. Laser-induced boiling, which perturbs conventional pictures taken some milliseconds after the hologram, can probably be suppressed by either using film with higher sensitivity to reduce the required laser energy, and/or by stretching the laser pulse from presently 20 ns to about 1 μs. The high spatial optical resolution in large volumes due to holography offers us the possibility of searching for a direct verification of the existence of ν_τ and of studying neutrino production of charm and beauty at Tevatron energies.

Acknowledgements

We are greatly indebted to the entire BEBC operation and maintenance group, in particular to G. Bochaton, R. Gnavi, E. Rusconi, F. Schenk, R. Talbot, D. Voillat and W. Wilkens and to W.M. Smart (Fermilab) for the dedicated help in setting up our equipment in a very short time. We appreciate the pleasant collaboration with the main users of BEBC during our parasitic run. We thank Prof. Sven Hartmann of the Columbia University Radiation Laboratory both for invaluable early advice and encouragement and for supplying us with the pulsed high-power ruby laser used in this test. We thank Argonne National Laboratory for giving us an addition-

al ruby laser oscillator on loan and GTE Labs, Waltham, Mass. for their donation of a laser cavity and power supply. We thank F. Cook for the precise manufacturing of the aspheric lens. We are grateful to G. Linser, A. Minten, D.R.O. Morrison and H. Wenninger for their encouragement and support of this experiment. The financial help from CERN and NSF is also gratefully acknowledged.

REFERENCES

[1] M. Dykes, P. Lecoq, D. Güsewell, A. Hervé, H. Wenninger, H. Royer, B. Hahn, E. Hugentobler, E. Ramseyer and M. Boratov, Nuclear Instr. & Meth. 179 (1981) 487.

[2] A. Hervé, K.E. Johansson, P. Lecoq, P. Olivier, J. Pothier, L. Veillet, G. Waurick and S. Tavernier, Nuclear Instr. & Meth. 202 (1982) 417.

[3] W.T. Welford in Proceedings of the International Conference on Bubble Chamber Technology, Argonne National Laboratory, edited by M. Derrick, (1970) 1024;

W.T. Welford, Appl. Physics 5 (1966) 872.

[4] F. Eisler, Nucl. Instr. & Meth. 163 (1970) 105.

[5] F. Pouyat, Preliminary tests on holography in BEBC, Proceedings of the Workshop on Holographic Techniques and Applications, Strasbourg and CERN/EF 82-6 (1982).

[6] H. Bjelkhagen, F. Pouyat, P. Kasper, E.E. Miranda, R.L. Sekulin, W. Venus and L. Walton, Tests of High resolution two-beam holography in a model of the Big European Bubble Chamber (BEBC), Nucl. Instr. & Methods 220 (1983) 300.

[7] F. Pouyat, Objectif haute resolution pour BEBC, Internal Note CERN/EF/BEBC/OP-79, unpublished (1979).

[8] C. Baltay, M. Bregman, M. Hibbs, A. Schaffer, G. Harigel, F. Eisler, R. Cence, E.B. Brucker, T. Hart, Talk at BEBC Users Meeting, CERN (November 1982), and

R. Cence, University of Hawaii, Internal Report JR-85-82 (1982).

[9] W.T. Welford, Bubble and spark chambers, vol. 1, edited by R.P. Schutt, Academic Press New York and London (1967) 234.

[10] G. Harigel, H.J. Hilke, G. Linser, F. Schenk, Nucl. Instr. & Meth. 188 (1981) 517.

[11] F.H. Poesposoetjipto, E. Hugentobler, Helvetica Physica Acta, 43 (1970) 203.

[12] R.C. Stamberg, D.E. Gillespie, J. Applied Physics 37 (1966) 459.

[13] G. Linser, Private communication.

[14] G. Harigel, G. Horlitz and S. Wolff, DESY-Report 72/16 (1972).

[15] G. Horlitz, S. Wolff and G. Harigel, Nucl. Instr. & Meth. 117 (1974) 115.

REFERENCES (Cont'd)

[16] G.A. Janusonis, Photographic Science and Engineering, Vol 22, No. 4 (1978) 297;

L.F. Costa, G.A. Janusosis and J.A. Merrigan, ibid. Vol. 22, No. 4 (1978) 301;

H. Bjelkhagen, Holographic recording materials and the possibility to increase their sensitivity, CERN/EF 84-7 (1984).

[17] M.W. Peters, University of Hawaii, HEPG Report UH-511-512-83 (1983).

[18] J.D. Trolinger, Optical Engineering Vol. 14, No. 5 (1975) 383.

FIGURE CAPTIONS

Fig. 1 Geometrical scattering function $G(\alpha)$ for bubbles ($n_b = 1.0$) in neon-hydrogen ($n_{Ne} = 1.085$), and for glass beads ($n_G = 1.5$) in air ($n_a = 1.0$).

Fig. 2 General layout of BEBC with its modified in-line holography equipment:

(1) Ruby laser on optics bench
(2) Dielectric mirror (Matra)
(3) Alignment device
(4) Vacuum tank window (Homosil)
(5) Vacuum tube inside general vacuum tank
(6) Double windows on chamber (Homosil)
(7) Dielectric mirror (Balzers)
(8) Aspheric light diverging lens
(9) Fisheye window
(10) Film platen
(11) Camera
(12) Pressurized porta-camp
(13) Vacuum tank of the chamber
(14) Interior of bubble chamber
(15) Floating disc with Scotchlite
(16) Expansion piston
(17) Expansion motor
(18) Movable platform
(19) Access shaft
(20) Magnet
(21) Iron shielding

Fig. 3 Ruby laser on the optics bench:

HN 2 mW Ne-He laser for alignment
RM Rear mirror (100% reflectivity)
Q Q-switch (K-QS2 Pockel cell)
MS Mode selector (Ø = 1.5, 1.8, 2.0 mm)
R Ruby rod (Ø = 3/8", L = 4")
IE Intracavity etalon (3 plates)
OE Output etalon (Ø = 10 mm, 70% reflectivity)
A1 Amplifier no 1 (ruby rod Ø = 3/8", L = 4")
BE1 Beam expander no 1 (magnification 2.67)
A2 Amplifier no 2 (ruby rod Ø = 9/16", L = 4")
A3 Amplifier no 3 (ruby rod Ø = 9/16", L = 4")
BE2 Beam expander no 2 (magnification 4)
A4 Amplifier no 4 (ruby rod Ø = 3/4", L = 8")
P Prism (60°, quartz)
HPM High power dielectric mirror (Matra).

FIGURE CAPTIONS (Cont'd)

Fig. 4 Angular distribution of the light intensity after the aspheric lens:

heavy line: design values for a parallel incoming beam of σ = 9.75 mm, quartz lens in liquid neon-hydrogen;

points: measured light distribution in air, at a distance of 200 cm incoming beam of $\emptyset$ = 30 mm, wavelength λ = 514 nm, continuous laser E = 100 mW;

crosses: measured data extrapolated to liquid neon/hydrogen.

Fig. 5 Measured light distribution of quartz lens: angle as function of diameter of incoming beam in air. Wave length λ = 514 nm, E = 100 mW.

Fig. 6 Layout for the measurement of the coherence length of the oscillator stage.

Fig. 7 Typical photo obtained with the layout shown in fig. 6.

Fig. 8 Target in warm BEBC, distance between parallel wires 3 mm:

(a) conventional photo;
(b) replayed hologram.

Fig. 9 Bubble chamber characteristics (schematic):

(a) dynamic pressure curve:

P_{st} = static pressure before expansion
P_{v} = vapour pressure
P_{sens} = pressure, at which sensitivity to ionizing particles is reached
P_{min} = minimum expanded pressure
t_{B} = time of beam injection
t_{L} = laser pulse (for holography)
t_{F} = flash (conventional pictures)

FIGURE CAPTIONS (Cont'd)

(b) bubble growth:
beam = bubbles along particle tracks
laser = laser induced parasitic bubbles.

Fig. 10 Real image of cosmic ray track, replayed through the fisheye windows with argon laser (λ = 514 nm):

(a) photographed on plate (approximately life size):
distance from centre of fisheye z_i = 300 cm in replay,
distance from axis x_i = 20 cm in replay.

(b) imaged by vidicon on TV-screen (Grundig, Newvicon, 625 lines, ϕ = 2/3", sensitivity 1.2 Lux max.), and photographed from screen (overall magnification of recording system: 24 x actual size).

Comparison of the same part of a track (approximately life size):

(c) real image on photographic plate,
(d) virtual image with vidicon (mirror symmetric to (c)).

Fig. 11 Microdensitometer measurements on track from replayed hologram (fig. 10(a)); values are scaled for wavelength and according to formulas in sect. 5:

(a) speed 1:50,
(b) speed 1:300.

Fig. 12 Dynamic pressure curves from BEBC expansions with neon-hydrogen filling (scales: 20 ms/division, 1 bar/division):

(a) without laser pulse,
(b) with laser pulse.

FIGURE CAPTIONS (Cont'd)

Fig. 13 (a) The arrangement of BEBC optics on a regular pentagon. The position of the light diverging lens and the projection of the light cone are shown schematically.

(b) Laser induced boiling in BEBC, photographed with conventional cameras (views 1, 3, 4 and 5) 8 ms after laser pulse.

Fig. 14 Experimental values of laser induced boiling in various bubble chambers and various wavelength. Energy versus pulse duration:

(1a) nitrogen laser in liquid nitrogen and argon (ABC test chamber) [10];

(1b) nitrogen laser in hydrogen (BEBC) [10];

(2) ruby laser in neon-hydrogen (BEBC) Q-switched, 20 ns, (this experiment):

(a) underneath aspheric lens,
(b) in beam plane; } heavy boiling

(3) spark gap in CF_3Br [11];

(4) ruby laser in CF_3Br [12];

(5) ruby laser in neon-hydrogen (BEBC) non-Q-switched, 1 ms, (this experiment):

(a) underneath aspheric lens,
(b) in beam plane. } no boiling observed

Fig. 15 Replay schemes for in-line holograms from BEBC, schematic:

(a) time-reversed real image with fisheye windows,

(b) virtual image with fisheye windows and telescope.

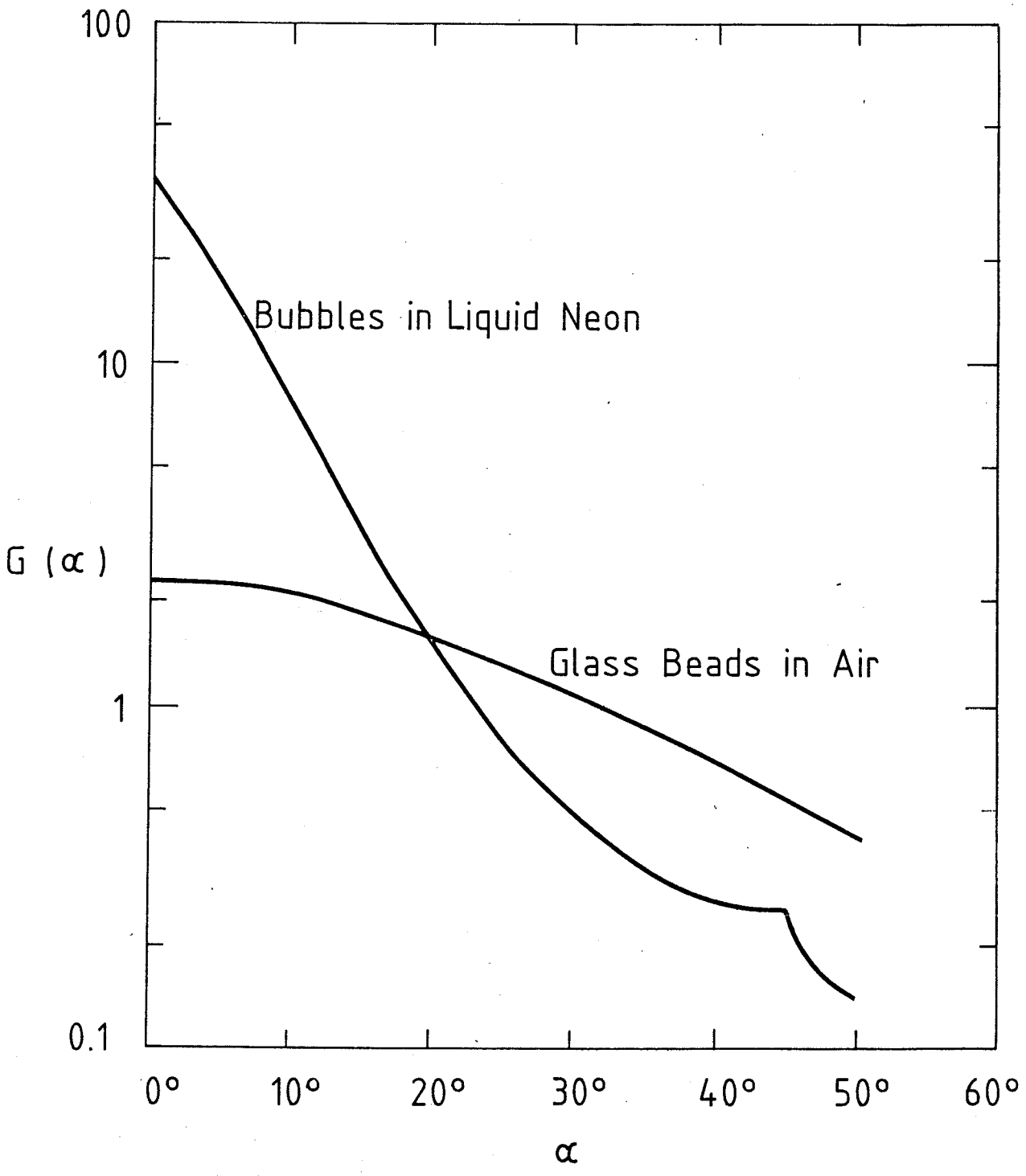
100
10
1
0.1
G (α)
Bubbles in Liquid Neon
Glass Beads in Air
0°
10°
20°
30°
40°
50°
60°
α

Fig. 1

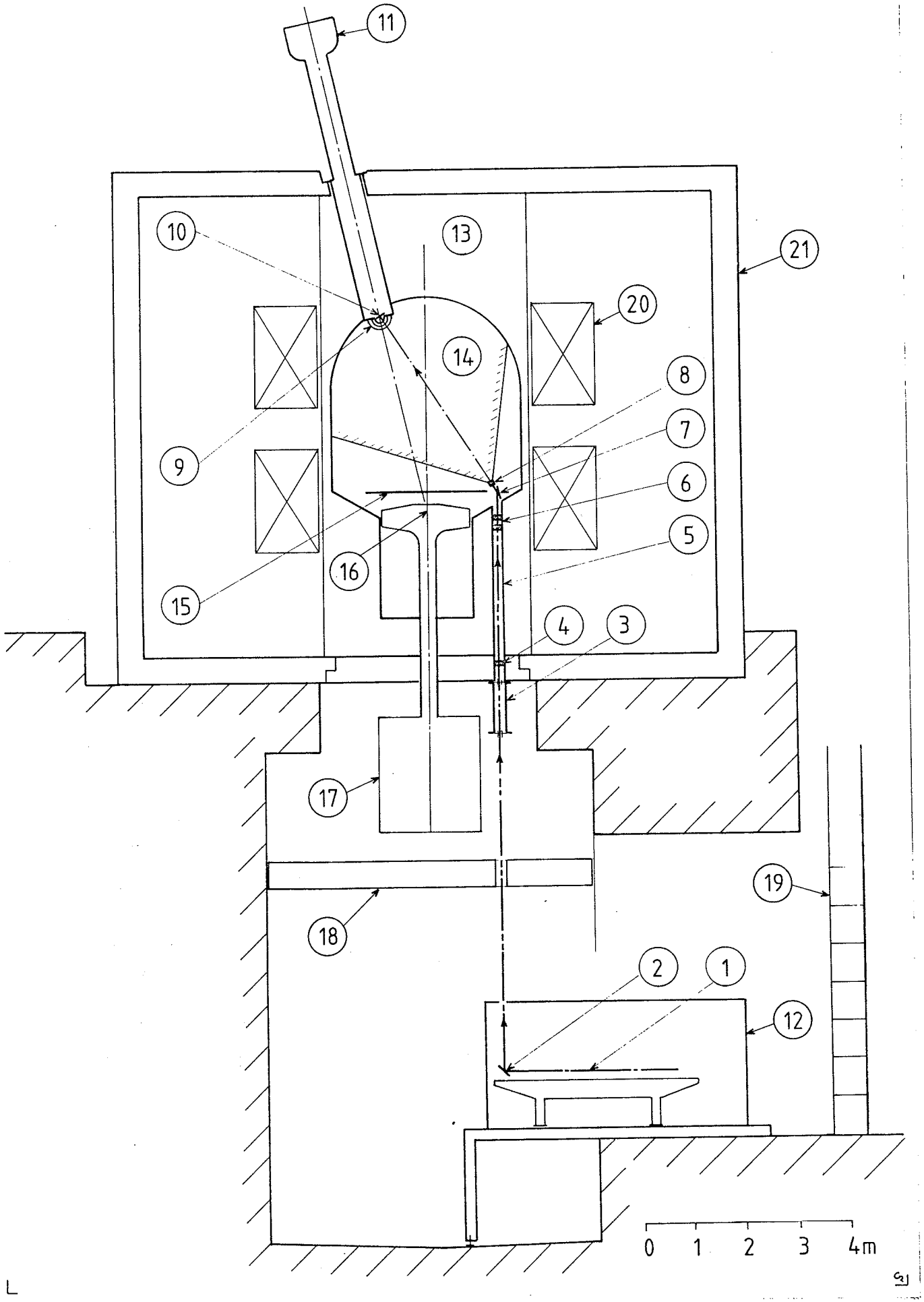

Fig. 2

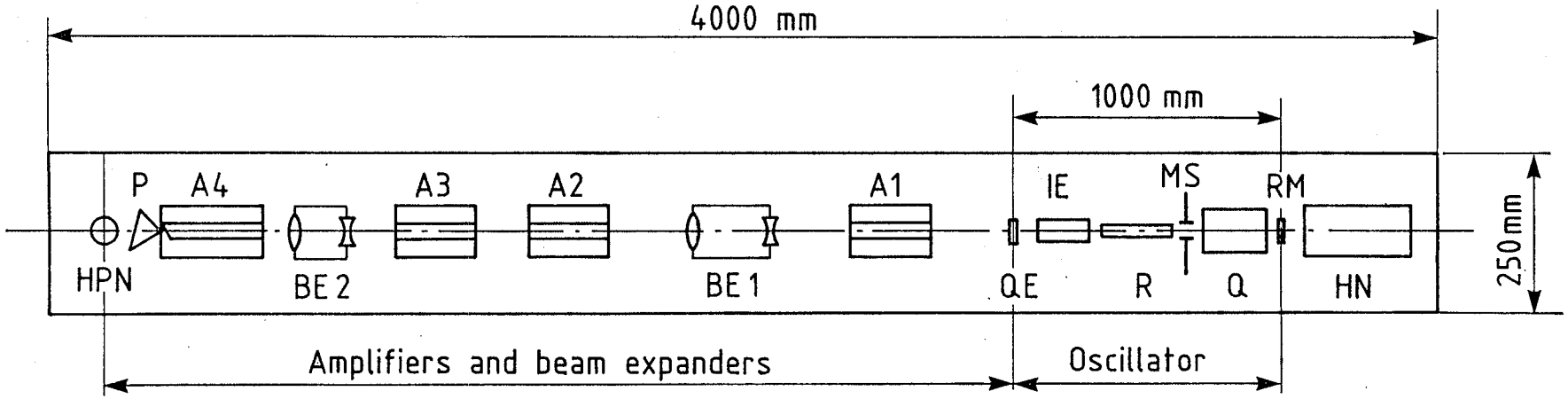
4000 mm
1000 mm
P
A4
A3
A2
A1
IE
MS
RM
HPN
BE 2
BE 1
QE
R
Q
HN
250 mm
Amplifiers and beam expanders
Oscillator

Fig. 3

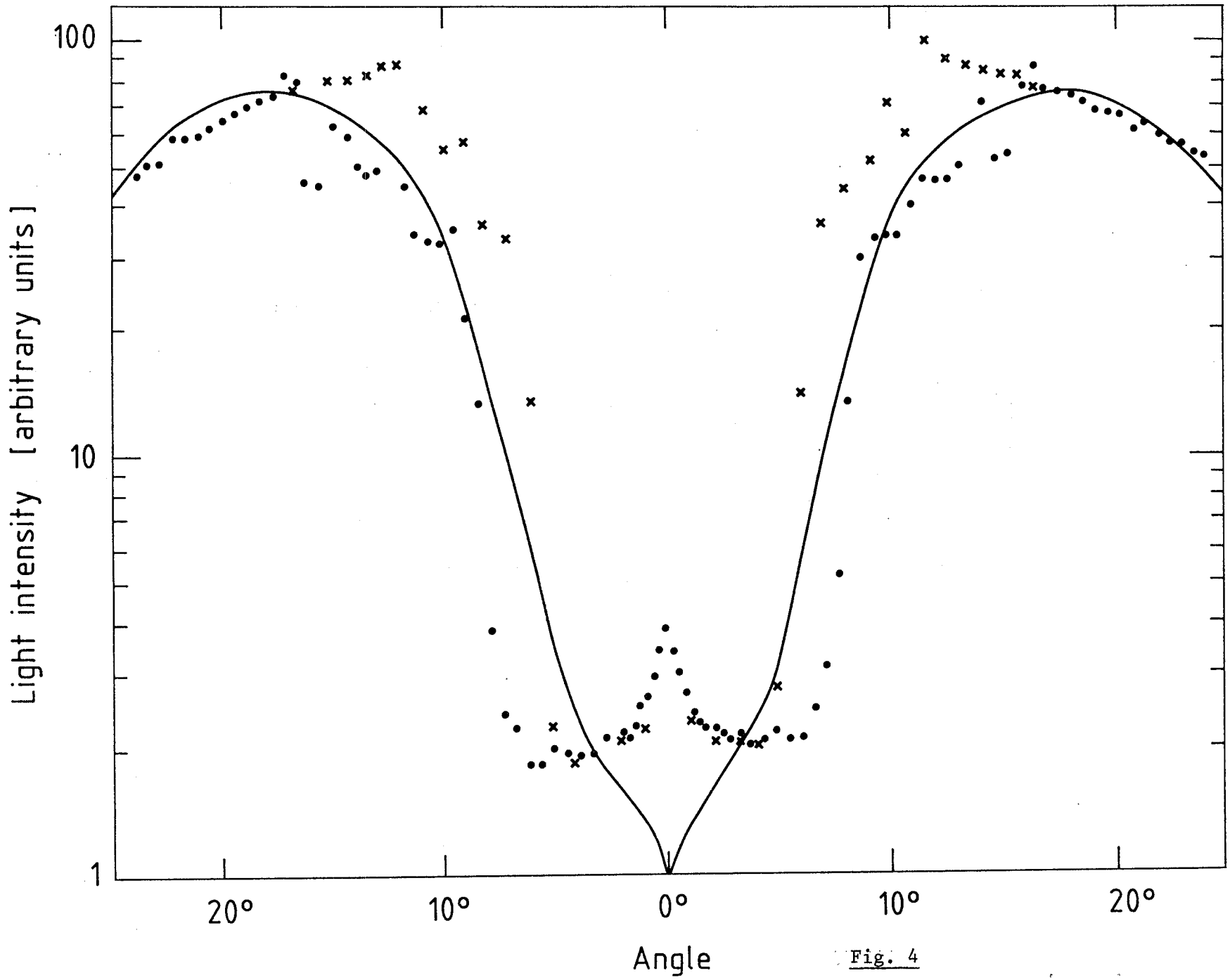

Fig. 4

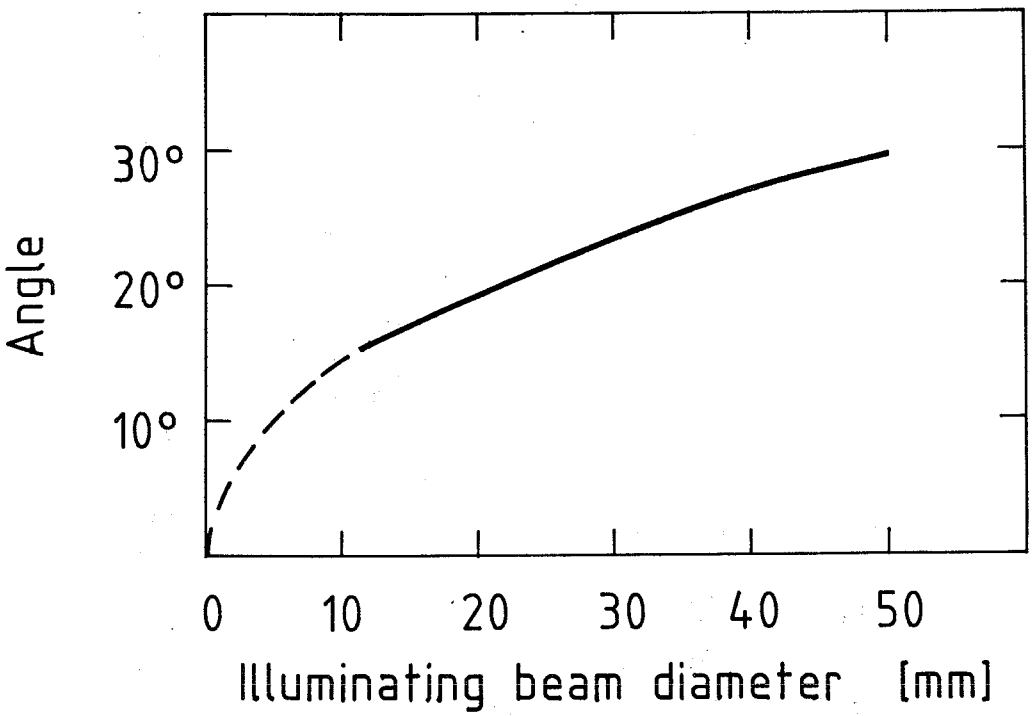

Fig. 5

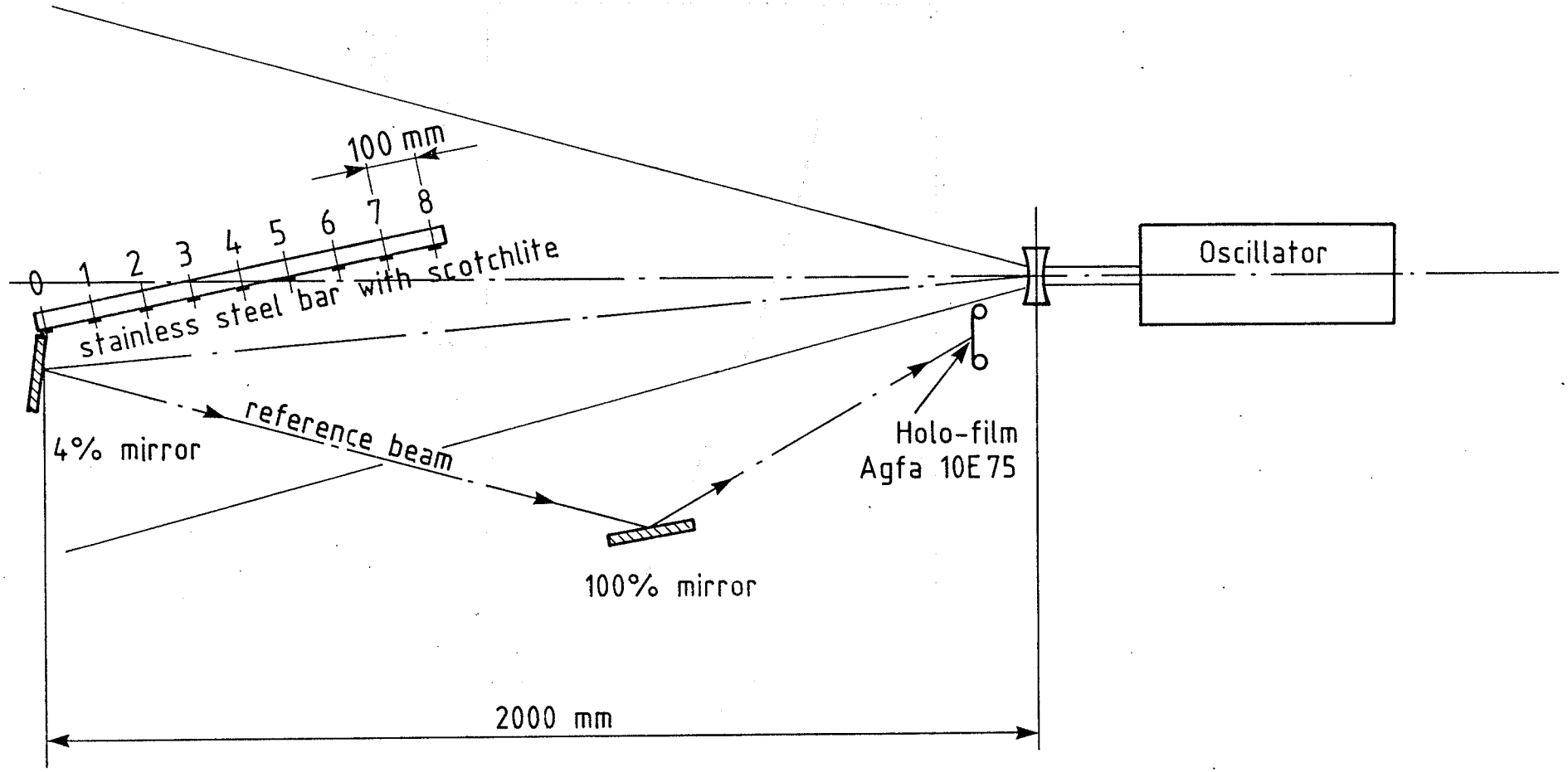
100 mm
0 1 2 3 4 5 6 7 8
stainless steel bar with scotchlite
Oscillator
reference beam
4% mirror
Holo-film
Agfa 10E75
100% mirror
2000 mm

Fig. 6

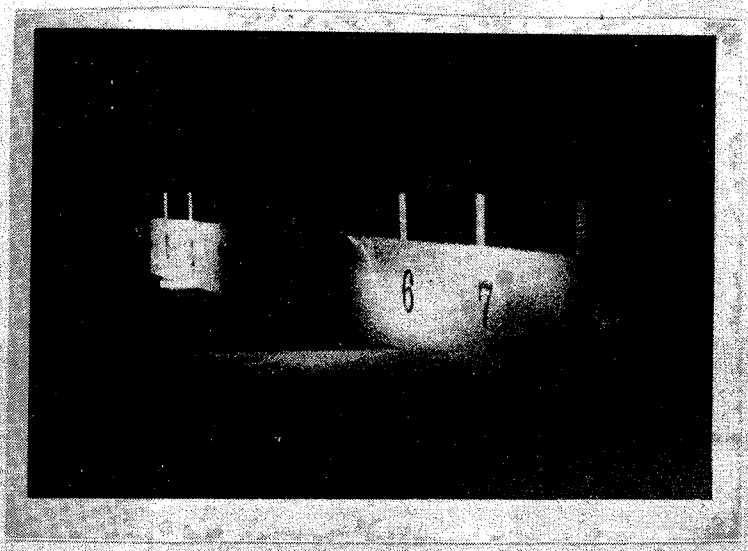

Fig. 7

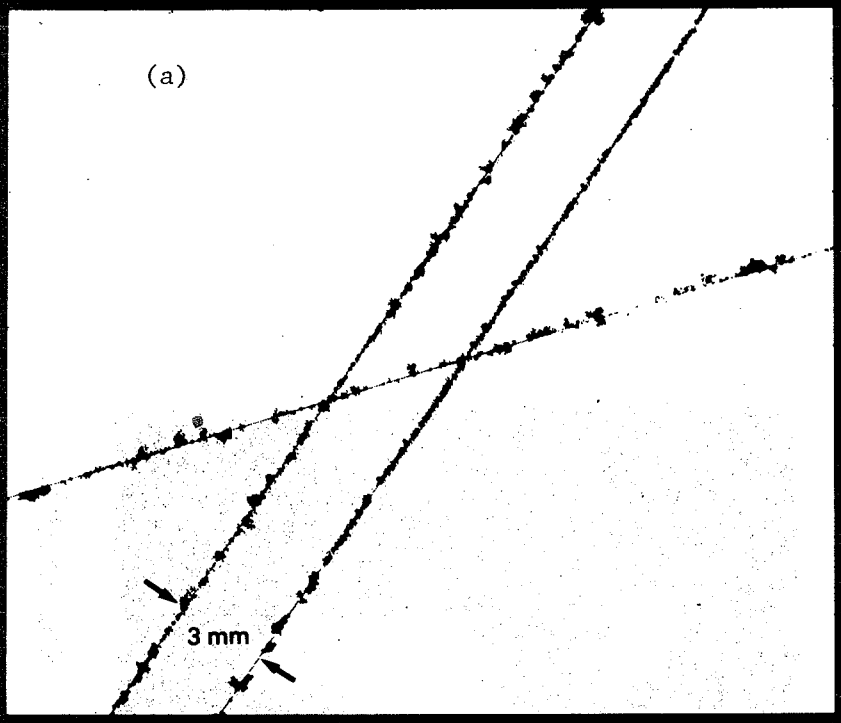

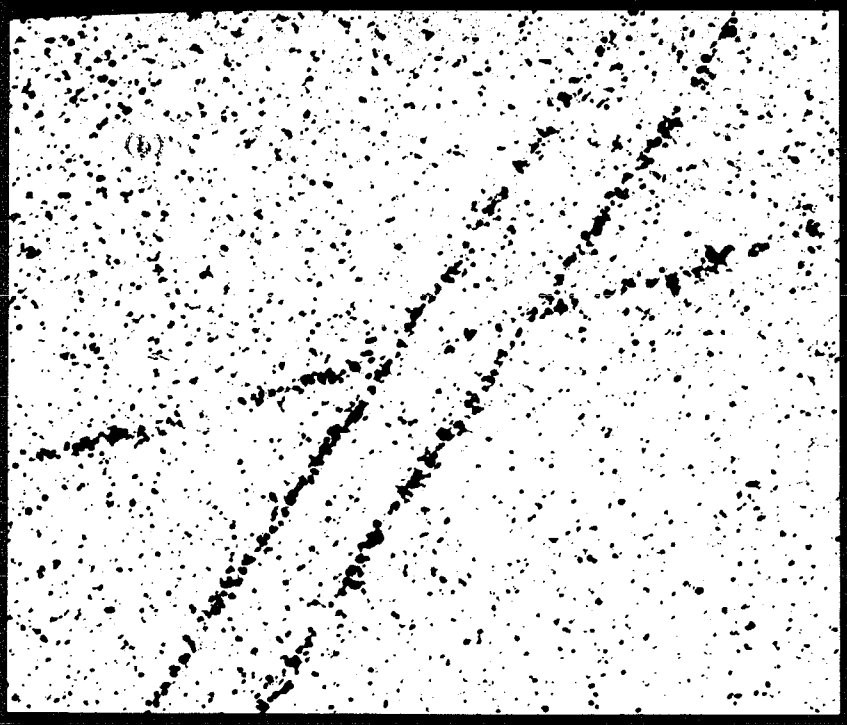

Fig. 8

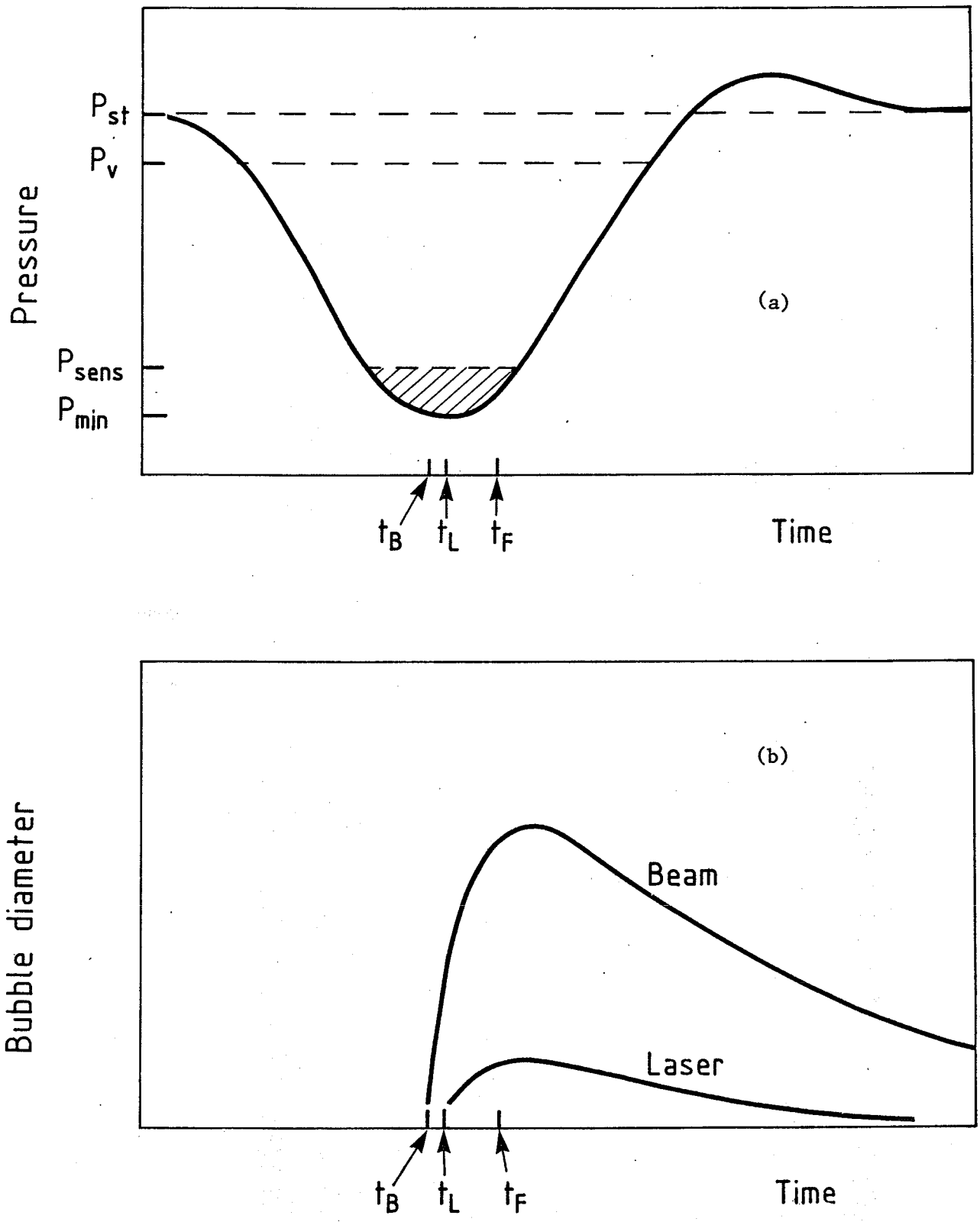
Pressure
P_{st}
P_v
P_{sens}
P_{min}
(a)
t_B
t_L
t_F
Time
Bubble diameter
(b)
Beam
Laser
t_B
t_L
t_F
Time

Fig. 9

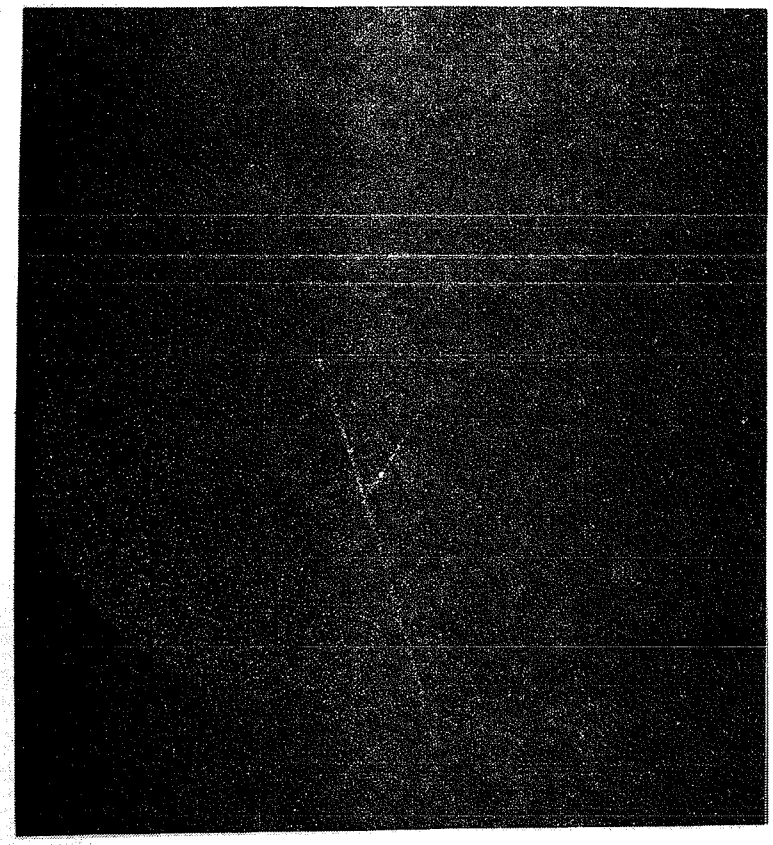

(a)

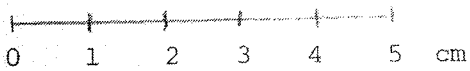

Real image, photographed on plate, ~life-size

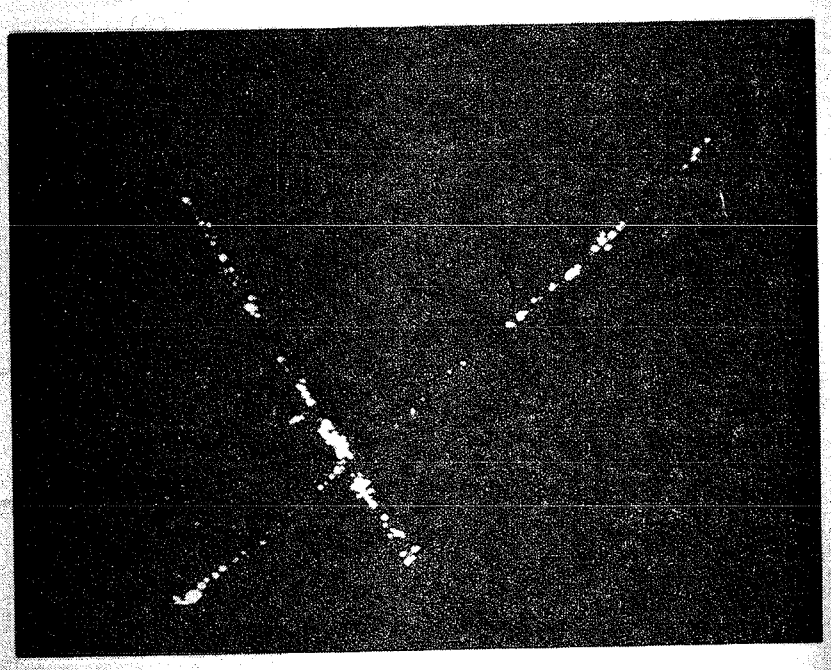

(b)

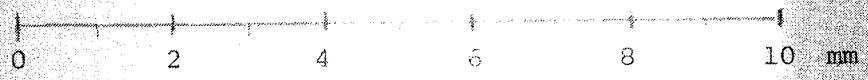

Real image, viewed by vidicon, ~10 x life-size

Fig. 10

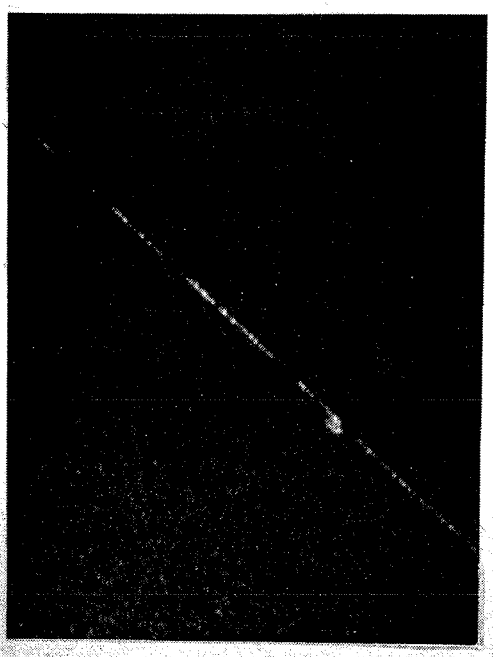

(c)

Real image, photographed on plate, ~life-size

SAME TRACK

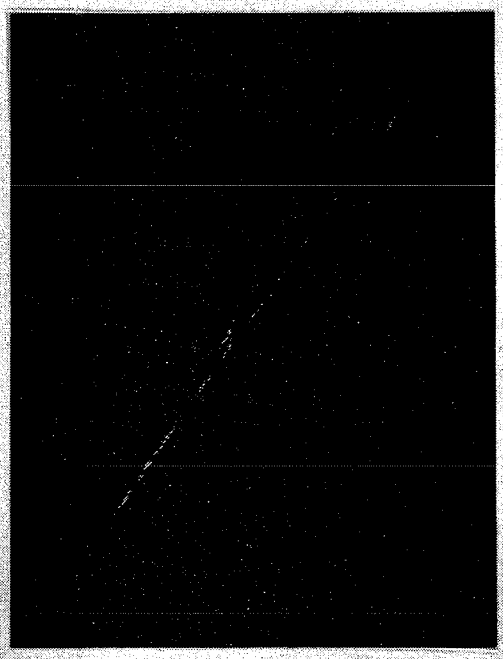

(d)

Virtual image, viewed by vidicon, ~ life-size

Fig. 10

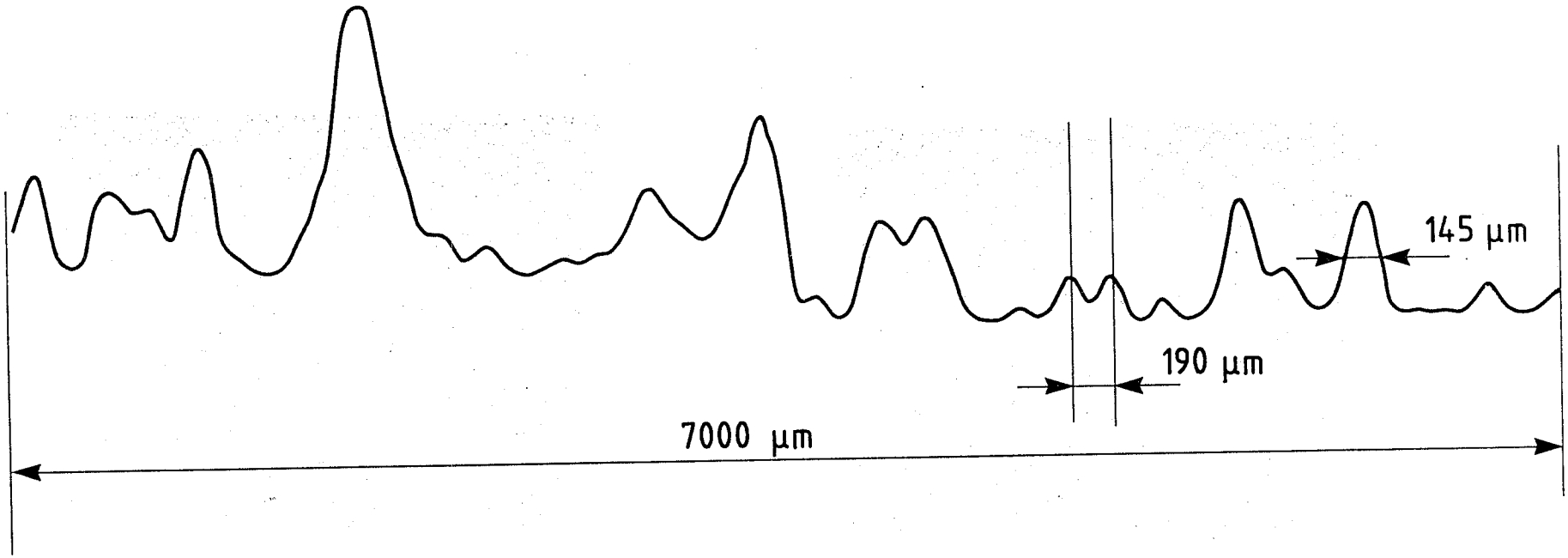

Fig. 11 (a)

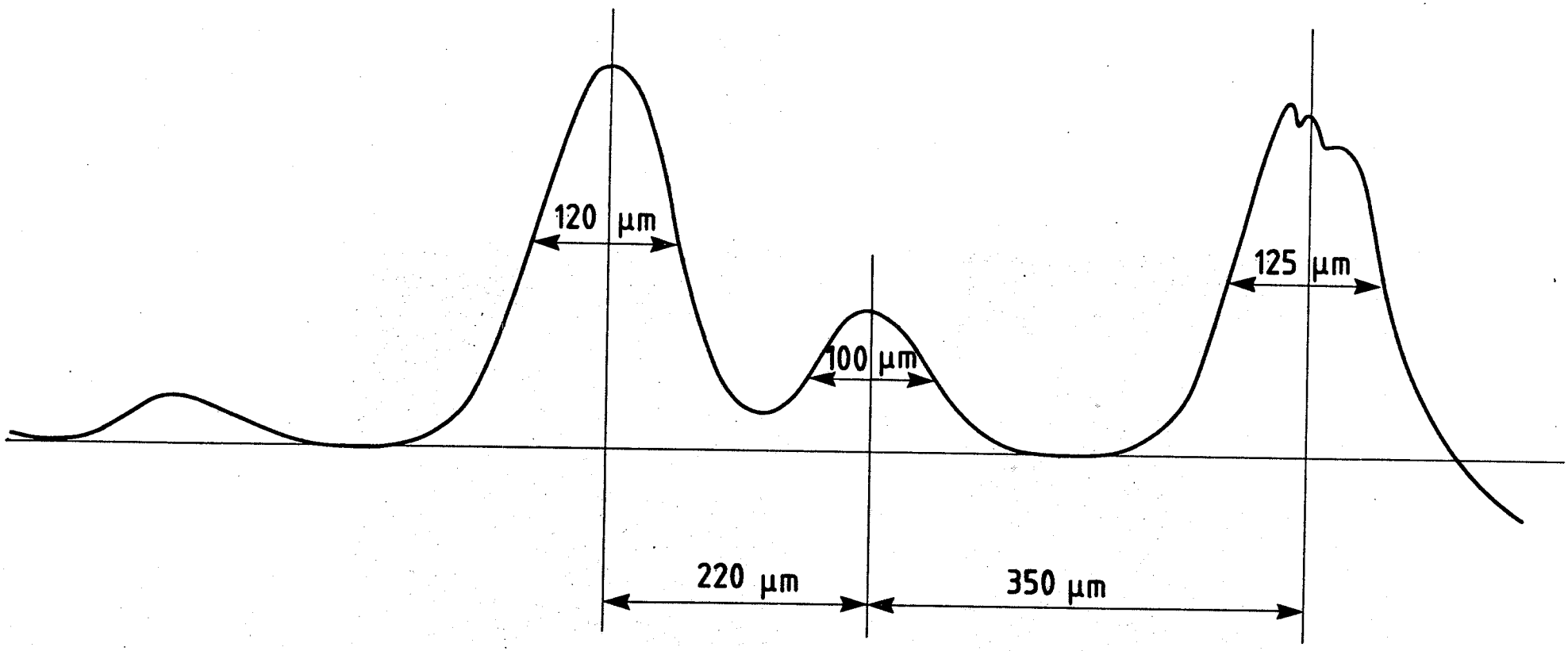

Fig. 11 (b)

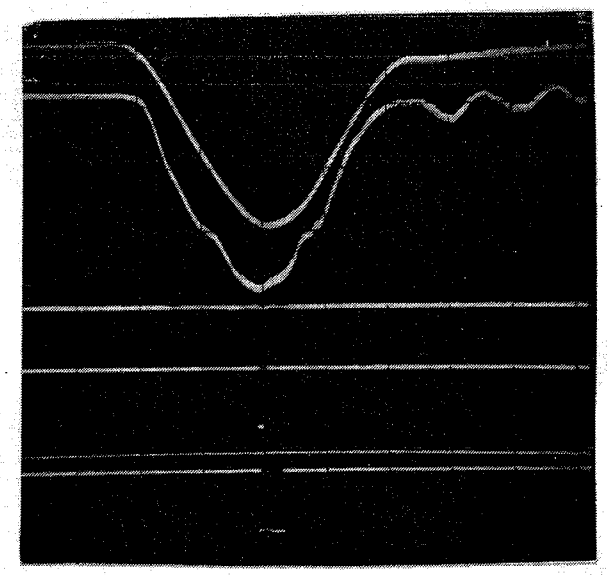

Piston stroke

Dynamic pressure

Flash delay

(a)

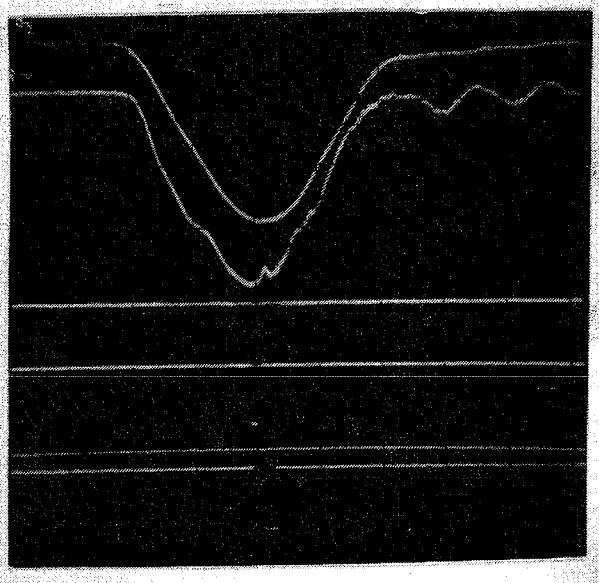

Piston stroke

Dynamic pressure

Flash delay

(b)

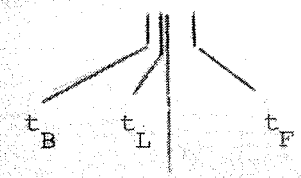

Pressure rise due to laser induced bubbles

Fig. 12

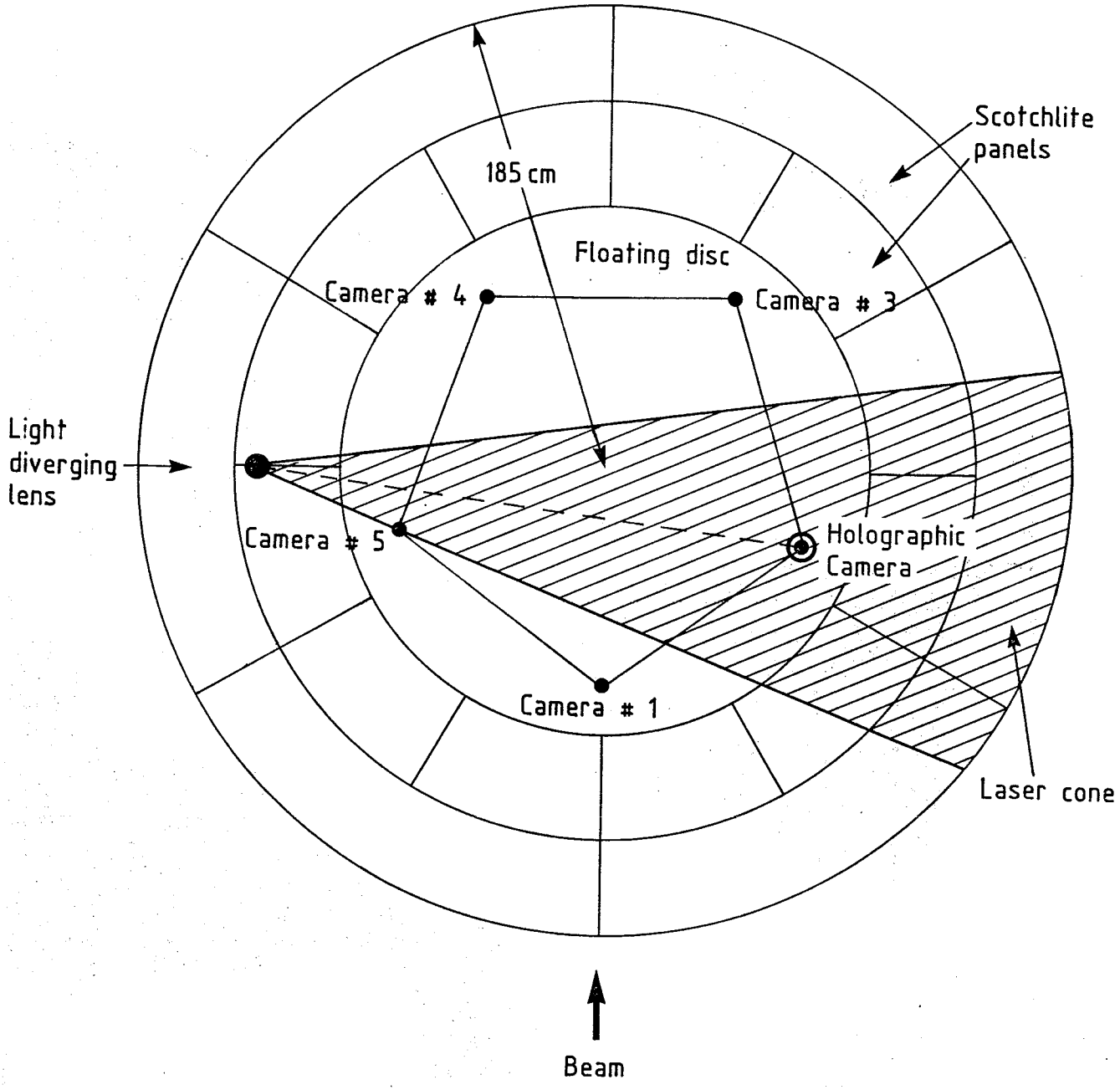
185 cm
Scotchlite
panels
Floating disc
Camera # 4
Camera # 3
Light
diverging
lens
Camera # 5
Holographic
Camera
Camera # 1
Laser cone
Beam

Fig. 13 (a)

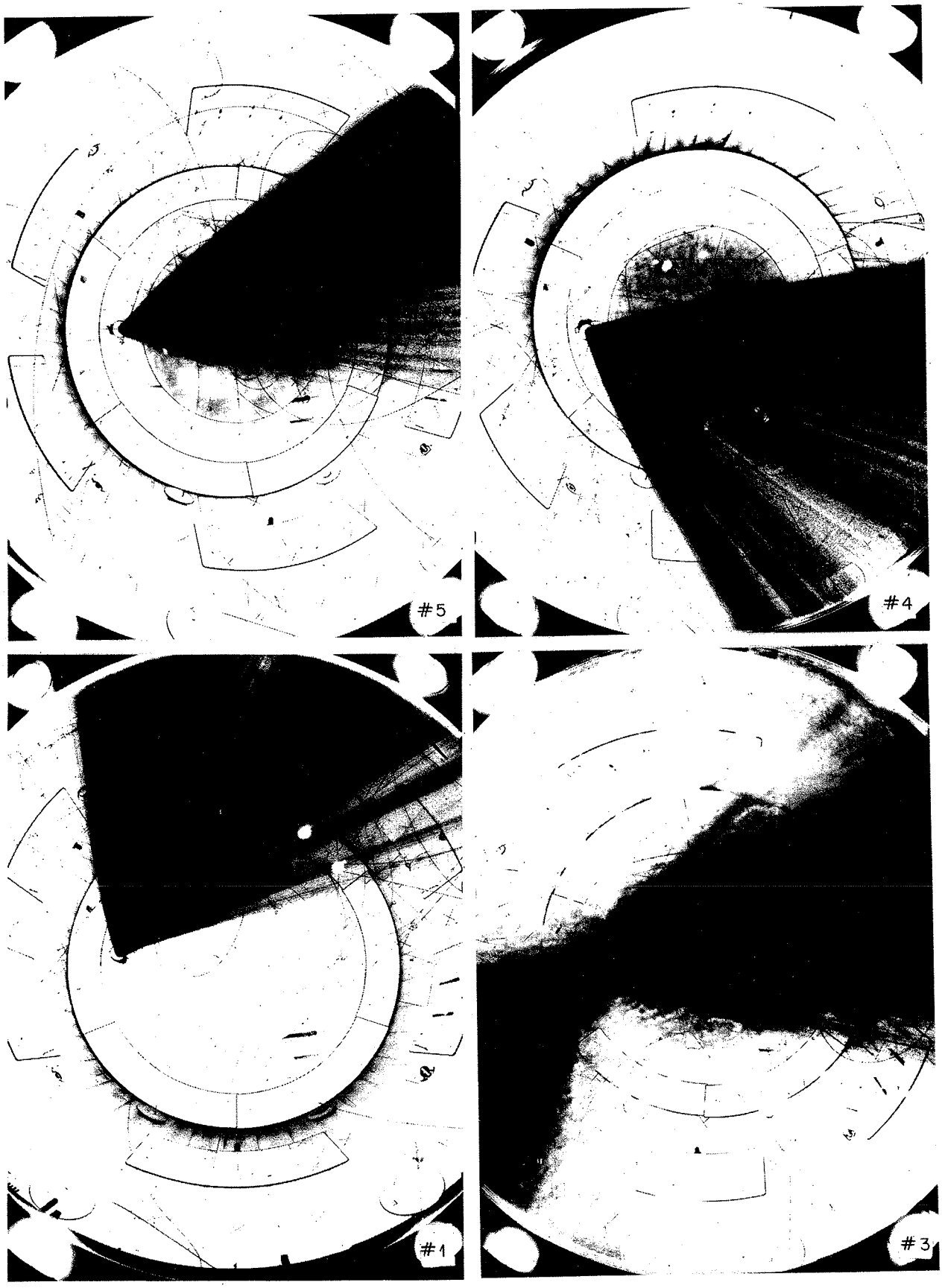

Fig. 13 (b)

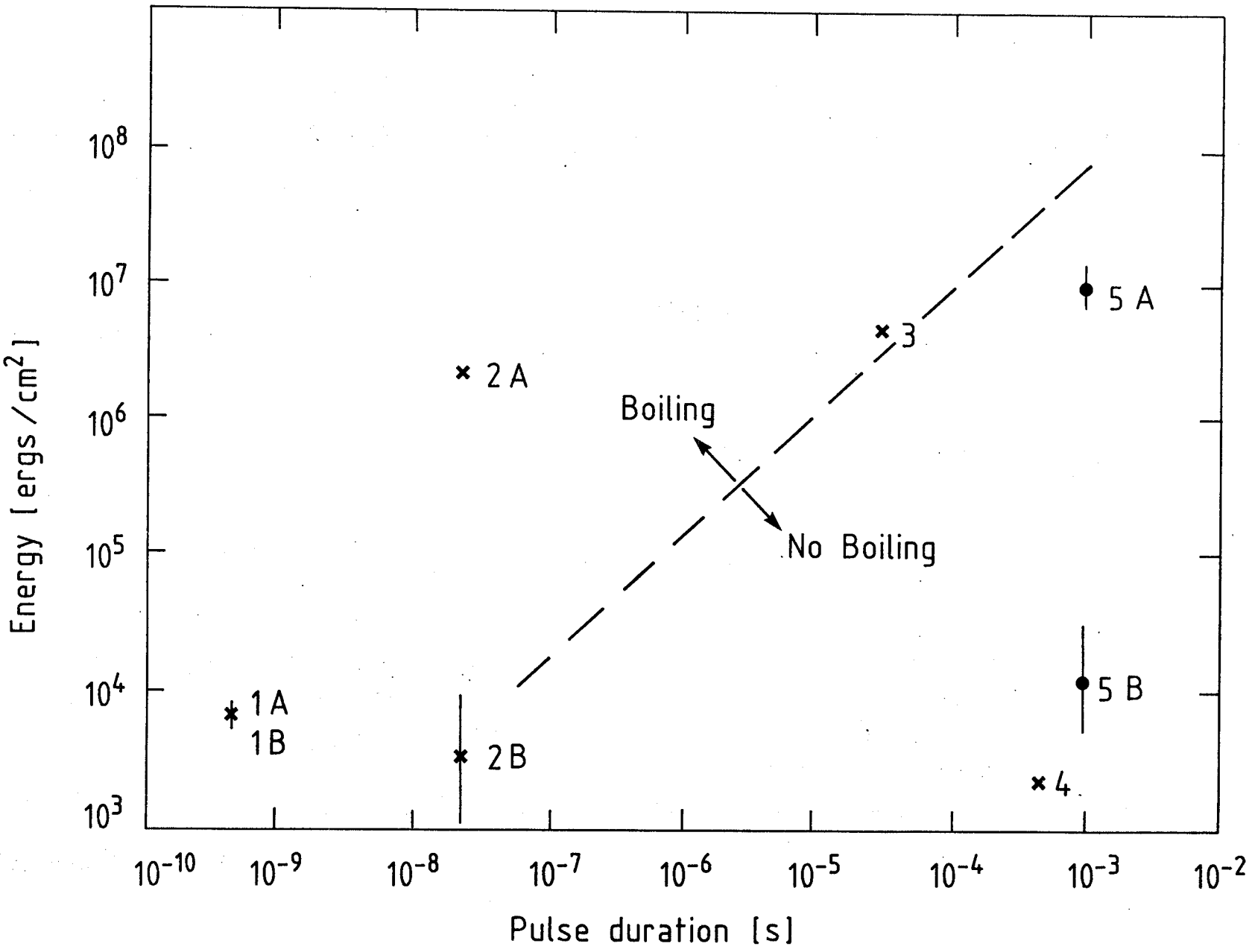
Energy [ergs/cm²]
10⁸
10⁷
10⁶
10⁵
10⁴
10³
1 A
1 B
2 A
2 B
3
4
5 A
5 B
Boiling
No Boiling
10⁻¹⁰
10⁻⁹
10⁻⁸
10⁻⁷
10⁻⁶
10⁻⁵
10⁻⁴
10⁻³
10⁻²
Pulse duration [s]

Fig. 14

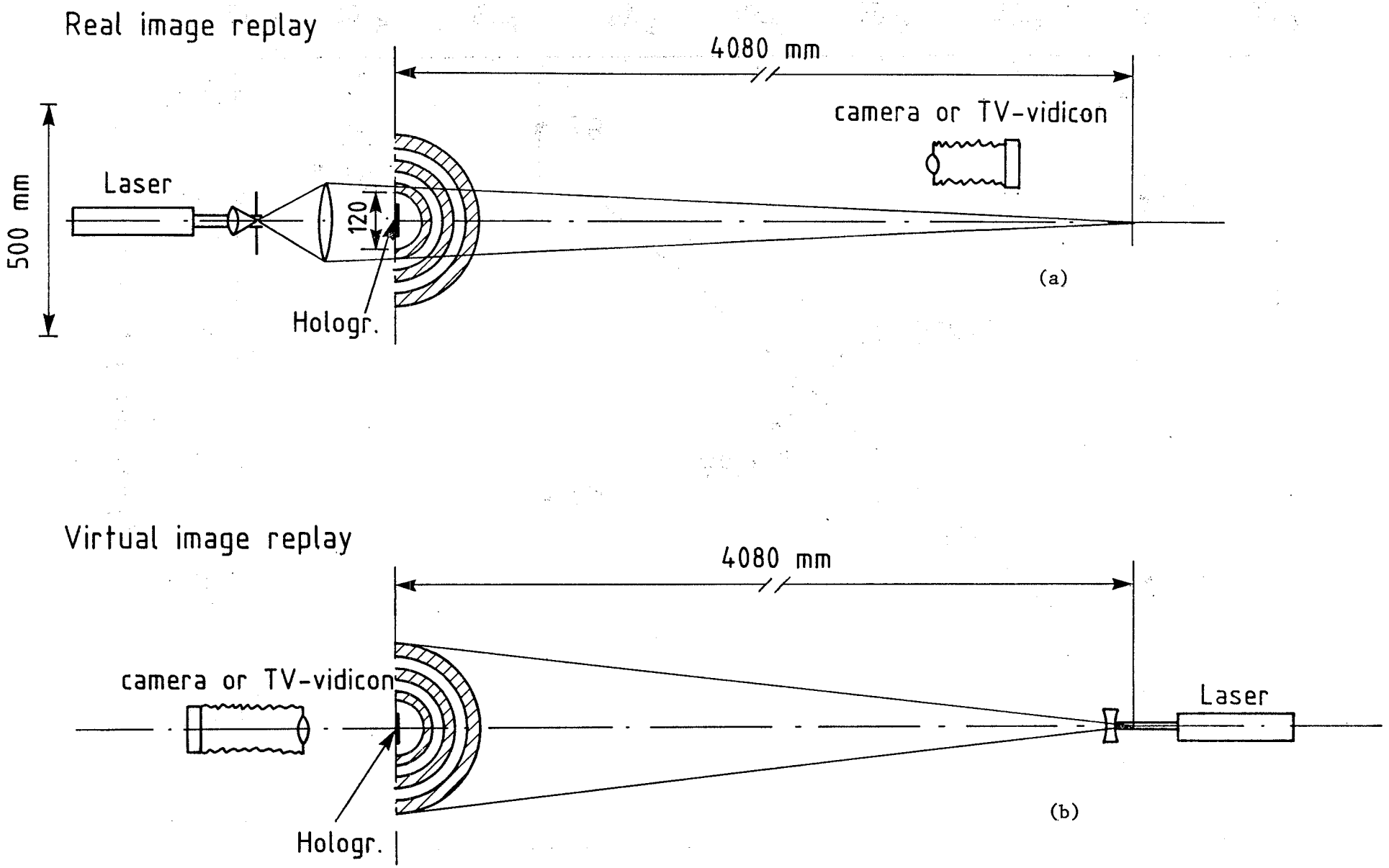
Real image replay
4080 mm
camera or TV-vidicon
500 mm
Laser
120
Hologr.
(a)
Virtual image replay
4080 mm
camera or TV-vidicon
Laser
Hologr.
(b)

Fig. 15